AN EXPERIMENTAL AND THEORETICAL INVESTIGATION OF SCATTERING BY FINITE PERFECTLY CONDUCTING CYLINDERS WITH VARYING CROSS-SECTION

KRISHNA M. PASALA, PH.D.
University of Dayton
Electrical Engineering Department
Dayton, Ohio 45469-0226

CARLOS R. ORTIZ
Wright Labs
Wright Patterson AFB
Dayton, Ohio 45433-7408

ABSTRACT. In this paper we consider the problem of scattering from a class of three dimensional (3-D) targets which are finite cylinders but whose cross-section varies along the axis of the structure. We devise a technique wherein the solution to this 3-D problem is reduced to a sequence of two dimensional (2-D) problems. Solutions of 2-D problems are easier to obtain than the solutions of 3-D problems and further a variety of well established 2-D methods are available. This procedure results in a dramatic reduction in computational complexity and also makes the technique suitable for implementation on computers with highly parallel architectures. A number of targets with ogival and elliptical cross-sections were built and their back-scattered RCS was measured at 3, 6 and 10 GHz. Good agreement between computed and experimental results is obtained validating the technique described here.

1. INTRODUCTION

It is frequently of interest to compute the scattering from three dimensional (3-D) targets with rather arbitrary shape. While a number of numerical techniques exist [1]-[11] to solve two dimensional (2-D) problems efficiently, relatively few techniques are available to solve the 3-D problems. Some of the methods are based on integral equations such as the surface patch code [6], [7]; others are based on solving the Maxwell's equations directly as in the FD-TD method [8], [9]. Codes that consider bodies of revolution are also available [10], [11]. Inevitably, 3-D codes demand large amounts of CPU time of powerful machines even for targets that are of moderate size. In addition to numerical techniques, high frequency techniques such as GTD, UTD or PTD [12], [13] may be used advantageously in cases where the targets are electrically large and when the requisite diffraction coefficients are available. Diffraction coefficients are not always available, however, as when the target is made of a dielectric, for instance. By combining numerical techniques with asymptotic techniques in appropriate fashion, hybrid methods [14] are realized which may be used to solve a wider class of problems.

In this paper, we are interested in computing the scattered field from a class of 3-D targets which are finite cylinders but whose cross-section may vary along the axis of the structure [15]-[17]. The technique itself is valid for targets that are made of metal, dielectric or both, though, we are only interested in perfectly conducting targets for the present. While the target is 3-D, the induced currents are determined by solving a sequence of 2-D problems. Efficient numerical techniques and codes [4], [5] are available to solve these 2-D problems. The notion of using 2-D solutions to solve 3-D problems is often used in the context of GTD, except that the solutions in this case are analytic and are based on asymptotic approximations [12]. Kumar has solved the problem of radiation from tapered dielectric rod antenna [18], by using the known solution to the underlying 2-D problem. Lai et. al. [19] have determined the scattering from straight dielectric structures by solving the underlying 2-D problem.

A number of models were fabricated. Some of these models are thin while others are bulbous. Some models have sharp edges while others are rounded. Measurements of backscattered RCS were made on these targets at 3, 6 and 10 GHZ and for both horizontal and vertical polarizations. These measured results are compared with results predicted by the theory described in this paper. Overall, excellent agreement is obtained between computed and experimental results. A salient feature of the method is the numerical efficiency. Computations are typically carried out using a PC. One of the typical cases consists of a target that is approximately $30\lambda^2$ in surface area. To compute the monostatic backscattered RCS over a range of 180 different angles of incidence, the CPU time required, on a Zenith Z386/25 PC with Weitek co-processor, is under three minutes! It may also be noted that the algorithm described here is specially suited for implementation on a parallel machine with many processors because each of the 2-D problems may be solved by a separate processor simultaneously and independent of the other 2-D problems.

2. THEORY

In this section we describe a technique to obtain the induced currents on a frustum of arbitrary cross-section illuminated by a plane wave as shown in Fig. 1. We also

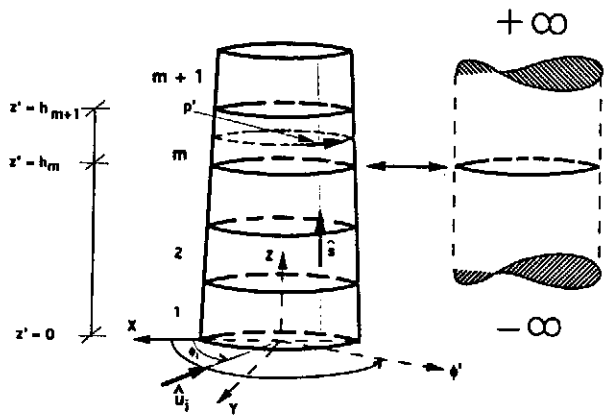

FIGURE 1. FRUSTUM OF ARBITRARY CROSS-SECTION

enumerate an efficient method to compute the field radiated by these induced currents. The frustum is divided into a number of electrically small blocks bounded by cross-sectional contours as shown in Fig. 1. Block numbered "m" is bounded by cross-sectional contours numbered "m" and "(m+1)". These contours need not be similar. The current on any contour, say the m^{th} contour, is taken to be the same as that on an infinitely long cylinder (shown with dashed line in Fig. 1) with the same cross section and subject to the same illumination. This is a 2-D problem and may be solved readily and efficiently. Thus, determining the current induced on a frustum is reduced to solving a sequence of 2-D problems. In order to determine the scattered field, we need to know the induced current at every point on the scatterer such as p' on the m^{th} block. This current is obtained, approximately, in terms of the current on the m^{th} contour. The details depend upon the polarization of the incident wave and we discuss here both the TM and TE polarizations.

2.1 TM Polarization: Induced Currents:

The electric field of the incident plane wave is parallel to the axis of the frustum and is given by,

$$\vec{E}_{inc} = E_0 \, e^{jk\rho\cos(\phi-\phi_i)} \, \hat{z} \quad . \tag{1}$$

E_o is the amplitude of the incident field, k is the propagation constant and ϕ_i is the angle of incidence. For an arbitrary observation point p', the current is given by,

$$\vec{J}(p') = J(\phi', z') \, \hat{s}, \quad h_m \le z' \le h_{m+1} \quad . \tag{2}$$

The unit vector $\hat{s}$ is as shown in Fig. 1. For an observation point p' that is on the m^{th} contour,

$$\vec{J}(p') = J_m(\phi') \, \hat{s} \, , \quad z' = h_m \quad . \tag{3}$$

For an observation point p' that is on the $(m+1)^{th}$ contour,

$$\vec{J}(p') = J_{m+1}(\phi') \, \hat{s} \, , \quad z' = h_{m+1} \quad . \tag{4}$$

The currents $J_m(\phi')$ and $J_{m+1}(\phi')$ are obtained by solving 2-D problems. For p' arbitrary, say on the m^{th} block ($h_m \le z' < h_{m+1}$), $J(\phi')$ remains unknown but may be approximated in terms of the known currents $J_m(\phi')$ and $J_{m+1}(\phi')$. Given that the m^{th} block is electrically small, the magnitude and phase of the current may be assumed to vary linearly between m^{th} and $(m+1)^{th}$ contours. This gives,

$$J(\phi') \approx |J_m(\phi')| \, e^{j(\psi_m + \delta\psi)} + \delta J \, e^{(\psi_m + \delta\psi)} \qquad h_m < z' < h_{m+1} \tag{5}$$

Where,

$$J_m(\phi') = |J_m(\phi')| \, e^{j\psi_m}$$

$$\delta J = \frac{\delta J_m}{\delta h_m} \left(z' - h_m \right)$$

$$\delta\psi = \frac{\delta\psi_m}{\delta h_m} \left(z' - h_m \right)$$

$$\delta J_m = |J_{m+1}| - |J_m|$$

$$\delta\psi_m = \psi_{m+1} - \psi_m$$

$$\delta h_m = h_{m+1} - h_m \tag{6}$$

In Equation (5), the change in magnitude δJ is quite small and may be neglected; however, the change in phase may not be neglected. Thus,

$$J(\phi') \approx |J_m(\phi')| \, e^{j(\psi_m + \delta\psi)} = J_m(\phi') \cdot e^{j\delta\psi} \quad . \tag{7}$$

According to Equation (7), the current on the contour through p' (refer to Fig. 1) may be taken to be the same as that on the m^{th} contour with the addition of the phase factor $e^{j\delta\psi}$. The change in phase $\delta\psi$ may be computed from Equation (6). It is highly desirable to find a closed form expression for $\delta\psi$. This may be accomplished if one assumes that $\delta\psi$ is simply the difference in the phase of the

incident field on the mth contour and the contour through p (dashed contour, Fig. 1). With this assumption, $\delta\psi$ is given by (refer to Fig. 2),

$$\delta\psi = k(\hat{u_i}\cdot\hat{\rho})\, d(z') \quad . \tag{8}$$

The vector $\hat{u_i}$ is the unit vector in the direction of propagation and is given by,

$$\hat{u_i} = -\cos\phi_i\,\hat{x} - \sin\phi_i\,\hat{y} \quad . \tag{9}$$

Also, as shown in Fig. 2,

$$\begin{aligned} d(z') &= \rho'_m(\phi') - \rho'(\phi') \\ &= (z' - h_m)\tan\gamma(\phi') \end{aligned} \tag{10}$$

and is a measure of the taper of the mth block at $\phi = \phi'$. Finally, the current is given by,

$$J(\phi') = J_m(\phi')\cdot e^{jk(\hat{u_i}\cdot\hat{\rho})\,d(z')} \quad . \tag{11}$$

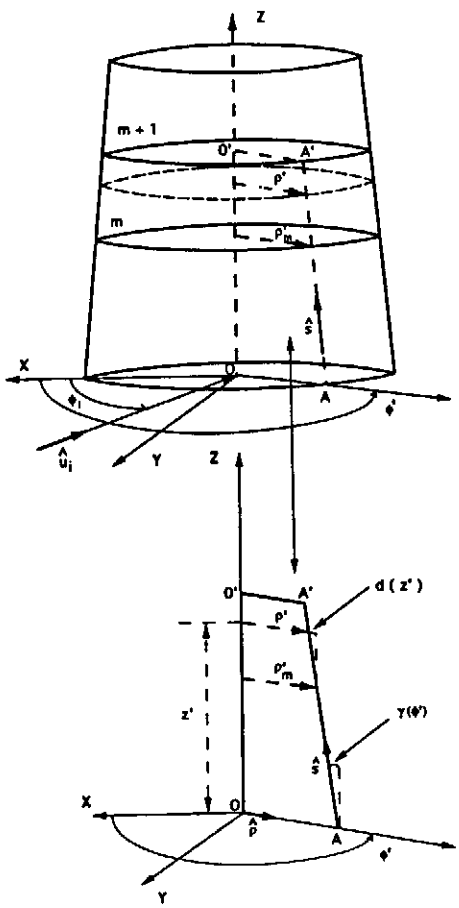

FIGURE 2. GEOMETRY FOR EVALUATING PHASE FACTOR

2.2 TM Polarization: Scattered Field:

The z-component of the scattered field from the mth block, E_{zm} is given by,

$$E_{zm} = -jk\eta \int_{\phi'=0}^{2\pi}\int_{z'=h_m}^{h_{m+1}} \left[\hat{z}\cdot\vec{J}(p')\right]\frac{e^{-jkr}}{4\pi r}\,da'$$

$$= -jk\eta \int_{\phi'=0}^{2\pi}\int_{z'=h_m}^{h_{m+1}} J_m(\phi')\sec\gamma(\phi') \tag{12}$$

$$e^{jk(\hat{u_i}\cdot\hat{\rho})(z'-h_m)\tan\gamma(\phi')}\frac{e^{-jkr}}{4\pi r}\,\rho'(\phi')ds'd\phi' \cdot$$

In the far field, making the usual far field approximations, we obtain,

$$e^{-jkr} \approx e^{-jkr_o}\, e^{jk\rho_m\cos(\phi_0-\phi')} e^{-jk(z'-h_m)\tan\gamma(\phi')\cos(\phi_0-\phi')} \quad . \tag{13}$$

Note that,

r = distance from the source point to the observation point,
r_0 = distance from the origin to the observation point, and
ϕ_0 = azimuthal coordinate of the observation point.

Referring to Fig. 2, we obtain,

$$\rho'(\phi') = \rho'_m - (z'-h_m)\tan\gamma(\phi') \quad . \tag{14}$$

Let,

$$c_1 = \left[\hat{u_i}\cdot\hat{\rho} - \cos(\phi_0-\phi')\right]\tan\gamma(\phi') \tag{15}$$

and

$$F(\phi') = Sec\gamma(\varphi')\, J_m(\phi')\, e^{jk\rho_m\cos(\phi_0-\phi')} \quad . \tag{16}$$

Now, the scattered field from the mth block may be obtained as,

$$E_{zm} = -jk\eta\,\frac{e^{-jkr_0}}{4\pi r_0}\,I_{TM} \tag{17}$$

where,

$$I_{TM} = \int_{\phi'=0}^{2\pi} F(\phi')\rho'_m(\phi')d\phi' \int_{z'=h_m}^{h_{m+1}} e^{jkc_1(z'-h_m)}\,dz'$$

$$-\int_{\phi'=0}^{2\pi} F(\phi')\tan\gamma(\phi')d\phi' \int_{z'=h_m}^{h_{m+1}} (z'-h_m)e^{jkc_1(z'-h_m)}\,dz' \tag{18}$$

Note that in Equation (18), variations with respect to ϕ' and

z' are separated. Further more, integrations with respect to z' may be carried out in closed form to yield,

$$I_{TM} = \int_{\phi'=0}^{2\pi} F(\phi')\rho'_m(\phi')Q_1(\phi')\,d\phi'$$

$$- \int_{\phi'=0}^{2\pi} F(\phi')\tan\gamma(\phi')\,Q_2(\phi')\,d\phi' \quad . \qquad (19)$$

Where,

$$Q_1(\phi') = \delta h_m\, e^{jkc_1\frac{\delta h_m}{2}}\, \frac{\sin\left(kc_1\frac{\delta h_m}{2}\right)}{\left(kc_1\frac{\delta h_m}{2}\right)} \qquad (20)$$

and

$$Q_2(\phi') = \frac{\delta h_m}{jkc_1}\left[e^{jkc_1\delta h_m} - e^{jkc_1\frac{\delta h_m}{2}}\, \frac{\sin\left(kc_1\frac{\delta h_m}{2}\right)}{\left(kc_1\frac{\delta h_m}{2}\right)} \right] \qquad (21)$$

Thus, to compute the scattered field from the mth block, it is only necessary to carry out one numerical integration with respect to the azimuth. The scattered field from the target as a whole may be obtained by summing the field from all the blocks. The number of blocks are taken to be sufficiently large to yield a converged scattered field.

2.3 TE Polarization: Induced Currents:

For the TE polarization, the magnetic field of the incident plane wave is parallel to the axis of the cylinder and is given by,

$$\vec{H}_{inc} = H_0\, e^{jk\rho\cos(\phi-\phi_i)}\,\hat{z} \quad . \qquad (22)$$

At an observation point p' on the mth block, the induced current is given by,

$$\vec{J}(p') = J_m(\phi')\, e^{jk(\hat{u}_i\cdot\hat{\rho})d(z')}\,\hat{u}_\ell(\phi') \quad . \qquad (23)$$

The unit vector $\hat{u}_\ell(\phi')$ depends upon the azimuthal coordinate of the observation and is shown in Fig. 1. All other variables of interest in Equation (23) were previously defined in section 2.1. Note that, as before, $\delta\vec{J}$ is neglected in obtaining Equation (23).

2.4 TE Polarization: Scattered Field:

Using the far field approximations, the z-component of the scattered magnetic field due to the mth block, H_{zm}, may be expressed as,

$$H_{zm} = -jk\frac{e^{-jkr_0}}{4\pi r_0}\, I_{TE} \quad . \qquad (24)$$

Where,

$$I_{TE} = \int_{\phi'=0}^{2\pi} \left[\hat{r}_0 \times \hat{u}_\ell(\phi')\cdot\hat{u}_z\right] F(\phi')Q_1(\phi')\rho'_m(\phi')d\phi'$$

$$- \int_{\phi'=0}^{2\pi} \left[\hat{r}_0 \times \hat{u}_\ell(\phi')\cdot\hat{u}_z\right] F(\phi')\tan\gamma(\phi')Q_2(\phi')\,d\phi' \quad . (25)$$

The functions $F(\phi')$, $Q_1(\phi')$ and $Q_2(\phi')$ are defined in Equations (16), (20) and (21). The total scattered field may be obtained by summing up the contributions from all the blocks comprising the target.

3. EXPERIMENTAL WORK

In order to test the theory described in Section 2, a number of models which are finite cylinders with varying cross-section were built. Two basic cross-sectional shapes were adopted. These are the circular ogive and the ellipse. The ogival geometry leads to a target with edges while the elliptical cross-section is used to devise targets that simulate the behavior of rounded edges. While all the targets with ogival cross-section are chosen to be "thin" blade like targets, some elliptical targets are thin and others are bulbous. Thus, a variety of models were fabricated. Typical geometries of these models are shown in Fig. 3. These targets are completely characterized by specifying the five parameters, L_1, D_1, L_2, D_2 and H. In this study, the height, H, of all the targets is taken to be 18 cm, which is six wavelengths at 10 GHz. Different tapers are obtained by changing L_1, D_1 and L_2, D_2. It may be noted that the slant angle γ is a function of azimuth. In the case of elliptical targets, the ratio of minor to major axis, may be controlled to obtain a "thin" or "bulbous" target. Three ogival targets and four elliptical targets were built initially. However, for the sake of brevity we present here the results corresponding to three ogival cylinders and two elliptical targets. The nominal dimensions of these cylinders are listed in Table 1. The actual dimensions realized after the fabrication process are also given (in parentheses) in Table 1. It may be readily seen that there are discrepancies between the actual and nominal dimensions of the target. These discrepancies are due to the fabrication process used.

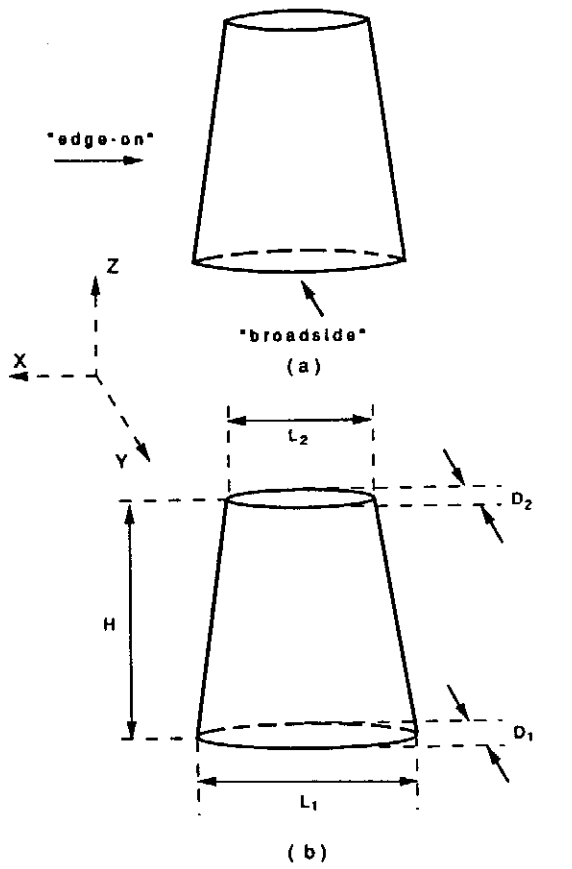

FIGURE 3. GEOMETRY OF TARGETS (a) OGIVAL CYLINDER (b) ELLIPTICAL CYLINDER

4. THEORETICAL AND EXPERIMENTAL RESULTS

The back scattered RCS of the five targets in Table-1 was measured in the Multi-Spectral Measurement facility at the Wright Patterson Air Force Base (WPAFB). These measurements were made at three different frequencies, 3,6, and 10 GHz, and also for both TE and TM polarizations. That is, a total of thirty scattering patterns were measured. Based on the theory presented here, scattering patterns were computed for each of these thirty cases. All the scattering patterns shown here are computed in the azimuthal plane because the measured patterns corresponded to this plane. However, the scattering pattern in any plane may be computed since the method determines the current on the target. The underlying 2-D problems of scattering by cylinders of arbitrary cross-section illuminated by TE and TM polarizations were solved by using the method of moments (MOM). The particular versions of the MOM and the corresponding codes are described in [4] and [5] for TE and TM polarizations respectively. The computed scattered field depends upon the number of blocks into which the target is divided. Numerical experiments are carried out to ensure the convergence of the scattered field as the number of blocks (of equal height) is increased. Indeed, good convergence is obtained and for the targets under consideration, a block size of about $\lambda/4$ or shorter appears to yield good results. All the computational results shown here are based on subdividing the target models into 24 blocks of equal height, which is a block size of $\lambda/4$ at 10 Ghz.

Table 1: Dimensions of Target Models

Model No.	Cross-Section	L1 Cm	D1 MM	L2 Cm	D2 MM	H Cm
O1	Ogive	7.5 (7.52)	6.3 (7.24)	6 (6.03)	5 (6.35)	18 (18)
O2	Ogive	8.7 (8.96)	7.5 (7.9)	6 (5.99)	5 (5.74)	18 (18.01)
O3	Ogive	9 (9.02)	7.5 (7.93)	6 (6.0)	5 (5.74)	18 (18)
E1	Ellipse	7.5 (7.48)	6.3 (6.81)	6 (5.98)	5 (5.74)	18 (18.01)
E2	Ellipse	9 (8.9)	22.5 (20.0)	6 (5.9)	15 (12.62)	18 (17.98)

We present here the results of both the theoretical and experimental work described. However, thirty scattering patterns are too many to be presented in a conventional fashion. Instead, the data has been presented in the form of five graphs, (Fig. 4 to Fig. 8) with each graph corresponding to one target. In order to accomplish this, the following conventions are used: All the targets are symmetric with respect to the "edge-on" angle of incidence and the "broad-side" angle of incidence. The edge-on angle of incidence is taken to be 0° and the broad-side angle of incidence is taken to be 90°. Hence, each of the Figs. 4-8 is divided into two parts where the region corresponding to 0°-90° corresponds to the TM polarization and the region corresponding to 90°-180° corresponds to the TE polarization. For each target and for each polarization, there are three different curves corresponding to the three frequencies. The RCS data corresponding to 6 GHz (σ_6) is plotted as is. The RCS data corresponding to 3 GHz (σ_3) is augmented by 15 dB and

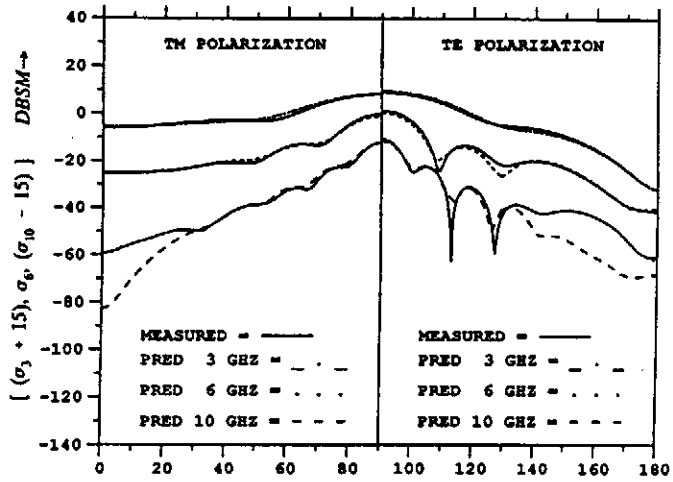

FIGURE 6. SCATTERING FROM OGIVAL CYLINDER NO. 3

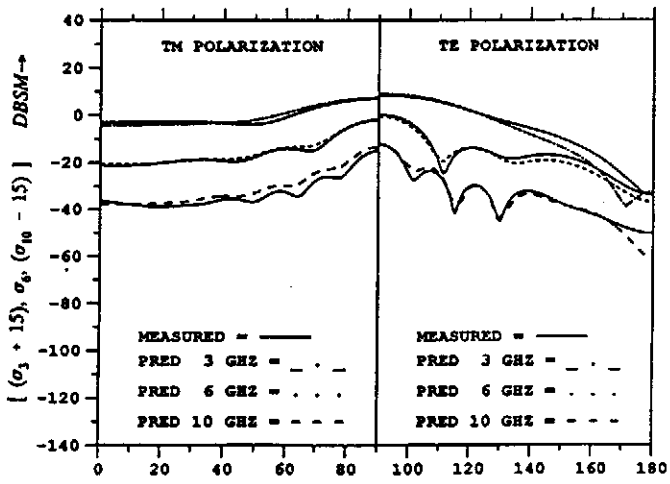

FIGURE 4. SCATTERING FROM OGIVAL CYLINDER NO. 1

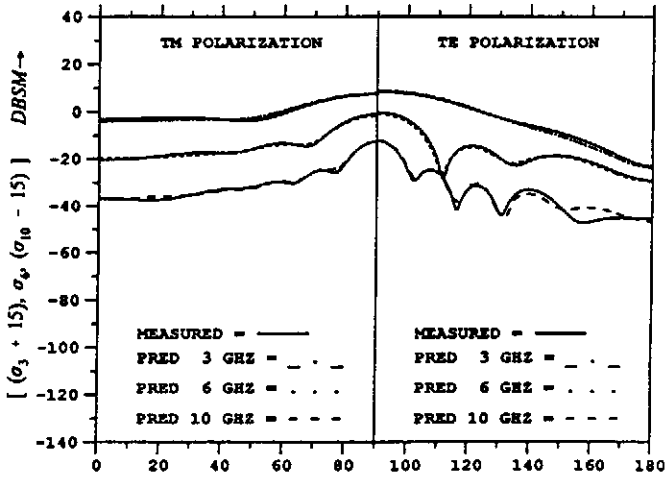

FIGURE 7. SCATTERING FROM ELLIPTICAL CYLINDER NO. 1

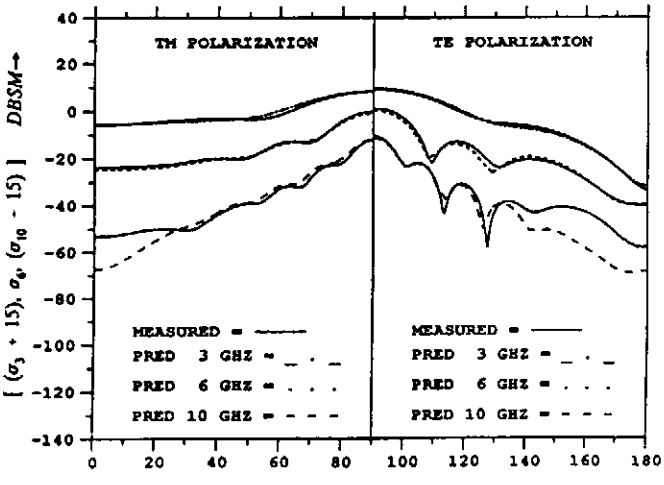

FIGURE 5. SCATTERING FROM OGIVAL CYLINDER NO. 2

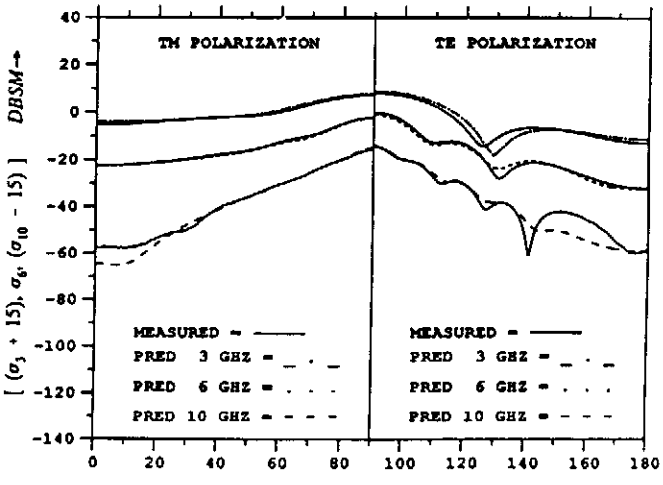

FIGURE 8. SCATTERING FROM ELLIPTICAL CYLINDER NO. 2

plotted, while the RCS data corresponding to 10 GHz (σ_{10}) is reduced by 15 dB and plotted. This procedure allows all three sets of data to be plotted on the same figure and assess the degree of agreement between the theoretical and measured data at the three frequencies simultaneously.

5. CONCLUDING REMARKS

In this paper we present an approximate but simple and computationally efficient technique to obtain the RCS of a class of 3-D targets. Scattering from any of the targets considered here may be readily computed using a PC. Not only is this technique computationally efficient, it places a minimum of demands on the memory required. It is only required to store the data necessary to compute the currents on one of the contours at a time. Once these currents have been used to compute the scattered field using Equation (19) or (26) for TM and TE polarizations respectively, these currents may be discarded and the memory cleared and used to compute scattering from the next block.

Our original intent of carrying out this investigation was to extend the use of the low frequency techniques like the method of moments into intermediate frequency region and for a class of commonly occurring 3-D targets. The technique has succeeded in doing so and appears to give useful results well into asymptotic region. It must be pointed out, though, that the technique is approximate. When the cylinders are straight the agreement is excellent. As the taper is increased and at the highest frequency, especially for edge-on angles of incidence, discrepancies occur as in Fig. 6. One possible reason is the difficulty of realizing a good edge in practice. The scattered field from the edge may be modelled by the field of a line source of travelling wave current located along the edge. Given that the length of this line source is larger than 6λ, at 10 GHz, it's scattered field has a very narrow beam and changes rapidly. A slight discrepancy in fabrication can result in tilting this pattern causing a rather large change in the measured field. Another possible reason is the breakdown of the assumption that the field of these targets is purely TE or TM, especially, for cases with the greatest taper (target-3 for instance). All of these may be a factor in the relatively large discrepancy seen in Fig. 6 for the edge-on angles of incidence.

The ansatz presented here is not limited to perfectly conducting targets, but may be readily extended to include penetrable, composite and coated targets. Investigations along these lines are discussed elsewhere [20], [21]. While we have used the MOM to solve the sequence of 2-D problems, one could equally well have used the FD-TD method or perhaps the finite elements method. Thus, the technique is quite flexible.

ACKNOWLEDGEMENT

We acknowledge the interest, help and encouragement of Dr. Gary Thiele. We gratefully acknowledge the support and encouragement of the Mission Research Corporation and Dr. Bill Kent in particular in carrying out the work reported here. The support of the Radar Branch, Avionics Mission Avionics Division, Wright Laboratory is acknowledged. The models were fabricated by the Fabrication Management Branch and the measurements were carried out at the Multi-spectrum Measurement facility at WPAFB.

REFERENCES

1. R. Mittra, *Computer Techniques for Electromagnetics*, New York, Hemisphere Publishing Co., 1987.

2. J.H.H. Wang, *Generalized Moment Methods in Electromagnetics*, New York, John Wiley & Sons, Inc., 1991.

3. J.A. Kong, *Finite Element and Finite Difference Methods in Electromagnetic Scattering*, New York, Pier 2, Elsevier Science Publishing Co., 1990.

4. D.T. Auckland, R.F. Harrington, "Moment Solution for Radiation and Scattering from Conducting Cylinders, TM Case," Syracuse University, Syracuse , New York, July 1975.

5. J.H. Richmond, "An Integral Equation Solution for TE Radiation and Scattering from Conducting Cylinders," NASA Contractor Report NASA CR-2245, April 1973.

6. S.M. Rao, D.R. Wilton, and A.W Glisson, "Electromagnetic Scattering by Surface of Arbitrary Shape," *IEEE Trans. Ant. Prop.*, Vol. AP-30, pp. 409-418, May 1982,

7. E.H. Newman and D.M. Pozar, "Electromagnetic Modeling of Composite Wire and Surface Geometries," *IEEE Trans. Ant. Prop.*, Vol. AP-26, pp. 784-789, Nov. 1978.

8. K.S. Yee, "Numerical solution of Initial Boundary Value Problems Involving Maxwell's Equations in Isotropic Media," *IEEE Trans. Ant. Prop.*, Vol. AP-14, No.3, pp. 302-307, 1966.

9. A. Taflove, K.R. Umashankar, "Review of FD-TD Numerical Modeling of Electromagnetic Wave Scattering and Radar Cross Section," *Proc. IEEE*, Vol. 77, No.5, pp. 682-699, 1989.

10. J.R. Mautz and R.F. Harrington, "Radiation and Scattering from Bodies of Revolution," App. Sci. Res., vol 20, p. 405, June 1969.

11. J.R. Mautz and R.F. Harrington, "An Improved E-field solution for a Conducting Body of Revolution," A.E.U, Band 36, p.198,1982.

12. P.H. Pathak, "Techniques for High-frequency Problems," Chapter 4 in *Antenna Handbook*, edited by Y.T. Lo and S.W. Lee, New York, Van Nostrand Reinhold Company, 1988.

13. J.B. Keller, "Geometrical Theory of Diffraction," *J. Opt. Soc. Am.*, Vol. 52, pp. 116-130, 1962.

14. G.A. Thiele, Overview of Selected Hybrid Methods in Radiating System Analysis," *Proc. IEEE*, Vol. 80, No. 1, pp. 66-78, January 1992.

15. J.M. Frederick, "Radar Signature of a Finite Ogive Cylinder," M.S.E.E. thesis, University of Dayton, Dayton, OH, August 1987.

16. C.R. Ortiz, "RCS of Arbitrary Finite Cylinders with Varying Cross-Section," M.S.E.E. Thesis, University of Dayton, Dayton, OH, April 1990.

17. K.M. Pasala, C.R. Ortiz, "Experimental and Theoretical Investigations on Scattering by Finite Cylinders with Varying Cross-section," IEEE-APS International Symposium Digest, Vol. 1, pp.180-183, Chicago, IL, July 1992.

18. A. Kumar, "Tapered Dielectric Rod Aerials," Ph.D. Thesis, Indian Ins. Sci., Bangalore, India, 1965.

19. A.K.Y. Lai, I.J. Gupta, W.D. Burnside, "Scattering by Dielectric Straps with Potential Applications as Target Support Structures," IEEE Trans. Ant. Propagat., Vol. AP-37, No.9, pp. 1164-1171, September 1989.

20. E.M. Friel, "Time and Frequency Domain Scattering by Dielectric Targets with Gently Varying Cross-Section," M.S.E.E. Thesis, University of Dayton, Dayton, OH, December 1992.

21. E.M. Friel, K.M. Pasala, "Scattering by Finite Cylindrical Dielectric Targets With Gently Varying Cross Section," IEEE-APS Symposium, Ann Arbor, MI, June 1993.